

LA-UR-21-23560 (Accepted Manuscript)

Engineering the beat phenomenon of quasi-Rayleigh waves for regions with minimal Surface Acoustic Wave (SAW) amplitude

Hakoda, Christopher Nobuo
Pantea, Cristian
Chillara, Vamshi

Provided by the author(s) and the Los Alamos National Laboratory (2021-09-13).

To be published in: Journal of Sound and Vibration

DOI to publisher's version: 10.1016/j.jsv.2021.116444

Permalink to record: <http://permalink.lanl.gov/object/view?what=info:lanl-repo/lareport/LA-UR-21-23560>

Disclaimer:

Los Alamos National Laboratory, an affirmative action/equal opportunity employer, is operated by Triad National Security, LLC for the National Nuclear Security Administration of U.S. Department of Energy under contract 89233218CNA00001. By approving this article, the publisher recognizes that the U.S. Government retains nonexclusive, royalty-free license to publish or reproduce the published form of this contribution, or to allow others to do so, for U.S. Government purposes. Los Alamos National Laboratory requests that the publisher identify this article as work performed under the auspices of the U.S. Department of Energy. Los Alamos National Laboratory strongly supports academic freedom and a researcher's right to publish; as an institution, however, the Laboratory does not endorse the viewpoint of a publication or guarantee its technical correctness.

Journal Pre-proof

Engineering the beat phenomenon of quasi-Rayleigh waves for regions with minimal Surface Acoustic Wave (SAW) amplitude

Christopher Hakoda , Cristian Pantea , Vamshi Krishna Chillara

PII: S0022-460X(21)00483-1
DOI: <https://doi.org/10.1016/j.jsv.2021.116444>
Reference: YJSVI 116444



To appear in: *Journal of Sound and Vibration*

Received date: 13 April 2021
Revised date: 16 August 2021
Accepted date: 7 September 2021

Please cite this article as: Christopher Hakoda , Cristian Pantea , Vamshi Krishna Chillara , Engineering the beat phenomenon of quasi-Rayleigh waves for regions with minimal Surface Acoustic Wave (SAW) amplitude, *Journal of Sound and Vibration* (2021), doi: <https://doi.org/10.1016/j.jsv.2021.116444>

This is a PDF file of an article that has undergone enhancements after acceptance, such as the addition of a cover page and metadata, and formatting for readability, but it is not yet the definitive version of record. This version will undergo additional copyediting, typesetting and review before it is published in its final form, but we are providing this version to give early visibility of the article. Please note that, during the production process, errors may be discovered which could affect the content, and all legal disclaimers that apply to the journal pertain.

© 2021 Published by Elsevier Ltd.

Engineering the beat phenomenon of quasi-Rayleigh waves for regions with minimal Surface Acoustic Wave (SAW) amplitude

Christopher Hakoda, Conceptualization, Methodology, Software, Validation, Formal analysis, Data Curation, Writing – original draft, Visualization^{a,*} chakoda@lanl.gov, Cristian Pantea, Conceptualization, Writing – review & editing, Supervision, Funding acquisition^a, Vamshi Krishna Chillara, Writing – review & editing^a

^aLos Alamos National Laboratory, Materials Physics and Applications, MS D429, Los Alamos NM 87545, USA

*Corresponding author.

Abstract

Surface Acoustic Waves (SAW) are prevalent in a variety of scientific fields. Typically, the ability to manipulate these surface waves has a significant impact on the efficacy of any SAW-based device. In this paper, we present a simple method for designing localized regions that have minimal SAW amplitude. These localized regions have valley-like drops in SAW amplitude and are achieved by using the spatial beat phenomenon of quasi-Rayleigh waves. Controlling the beat phenomenon allows us to manipulate where and how these localized regions appear in the waveguide. In particular, the localized regions can be designed to have variable widths and can be positioned consecutively due to minimal wave scattering. The design methodology and physics are described in detail, and several supplementary simulations are provided to demonstrate the efficacy of the proposed method. Lastly, we briefly discuss how the proposed approach could potentially be exploited to implement a localized high-pass filter and enables SAW wave propagation that avoids surface obstacles.

Keywords

SAW; surface acoustic wave; surface wave; quasi-Rayleigh wave; Rayleigh wave; beat phenomenon; Rayleigh-like wave;

1. INTRODUCTION

Surface Acoustic Wave (SAW) devices are prominently used in a variety of scientific fields and industrial applications. In microscale acoustofluidics, SAWs are used to influence the chemical, physical, or flow characteristics of a fluid or particles present in a fluid [1]. SAWs are also used in IF and RF filters. These SAW-based filters are better known as Acoustic Wave Filters, and are used due to their simplicity, low-cost, and effectiveness [2]. Radio Frequency Identification (RFID) tags are also known to use SAWs. In particular, passive RFID tags that use SAWs have been demonstrated to be long lasting, robust, and have a stronger return signal when compared to other Integrated-Circuit RFID tags [3].

The foundation for many of these devices can be traced back to the introduction of the Interdigital Transducer (IDT) in 1965 by White and Voltmer [4]. The design would be further refined over the years to manipulate the excitation of SAWs in application-specific ways (e.g., [5-7]). In the decade following the introduction of the IDT, many studies related to manipulating SAWs were published. These studies include designs for directional couplers [8, 9], strip waveguides [8, 10-12], ridge waveguides [13] and many other methods for manipulating surface waves [14, 15]. More recently, metamaterials have been studied for their ability to manipulate SAWs in new and efficient ways (e.g., [16, 17- 20]). Among the earlier methods for manipulating SAWs, Humphreys and Ash [21] introduced a scattering method for mode converting between SAWs and bulk waves. An implementation of this method allowed them to redirect SAWs from one surface to another in order to avoid obstacles on the surface of a plate. Given the many modern applications of SAWs that were mentioned previously, we could envision many scenarios where this capability would be useful.

Instead of using wave scattering as in [21], which can lead to increased noise and reduced transmission, we choose to exploit the characteristics of quasi-Rayleigh waves and investigate methods for achieving the same capability. Quasi-Rayleigh waves are not often used in research or industry. The only implementations of quasi-Rayleigh waves that the authors are aware of is in the fields of Structural Health Monitoring (SHM) and Non-Destructive Evaluation (NDE) [22-26]. In SHM and NDE, quasi-Rayleigh waves are used for remotely investigating potential structural damage in

difficult to reach locations. The quasi-Rayleigh wave's inherent spatial beat phenomenon is also used for avoiding obstacles or investigating surfaces that cannot be normally accessed.

In this paper, we present a simple method for designing acoustic waveguides with localized regions of minimal SAW amplitude. The method operates by exploiting a spatial beat phenomenon, which is characteristic of quasi-Rayleigh waves. The geometry and positioning of these regions is adjustable by strategically varying the thickness of the acoustic waveguide. Due to the physical phenomena involved, the method also results in minimal wave scattering and attenuation which allows for these localized regions to be positioned consecutively. Thus, this methodology gives SAW-wave practitioners another way of controlling the surface wave propagation in their devices, which could lead to new SAW devices and improving the efficacy of current SAW devices.

This article is organized as follows. Section II discusses the theory and concepts of quasi-Rayleigh waves and how they relate to SAWs. In Section III, the theory and methods for designing localized regions with minimal wave amplitude are detailed with example designs. Section IV presents simulation results that demonstrate the efficacy of the example designs under a variety of scenarios. Lastly, Section V briefly discusses the potential implementations of this method, which will be the subject of future research.

2. WHAT IS A QUASI-RAYLEIGH WAVE AND HOW DOES IT RELATE TO SURFACE WAVES?

Perhaps the most well-known SAW is the Rayleigh wave, which was first characterized by Lord Rayleigh in 1885 [27]. As Lord Rayleigh described it, Rayleigh waves are “waves upon the plane free surface of an infinite homogeneous isotropic elastic solid”. He goes on to describe the profile of the planar wave as being “confined to a superficial region, of thickness comparable with the wave-length” [27]. That is, the medium in which a Rayleigh wave travels is defined as a homogeneous elastic solid with isotropic material properties. The medium is semi-infinite, otherwise known as a half-space, and has a singular surface with traction-free boundary conditions. The Rayleigh wave is non-dispersive, which leads to a phase velocity (and group velocity) that can be calculated using the following equation,

$$c_R = c_S \frac{0.87 + 1.12\nu}{1 + \nu}. \quad (1)$$

Where c_S is the bulk shear wave speed and ν is the Poisson's ratio of the isotropic half-space [28]. An example displacement profile for a Rayleigh wave is shown in Figure 1. Although not shown in Figure 1, the displacement components are normally $\pi/2$ out-of-phase with each other which results in the Rayleigh wave's well-known elliptical particle motion.

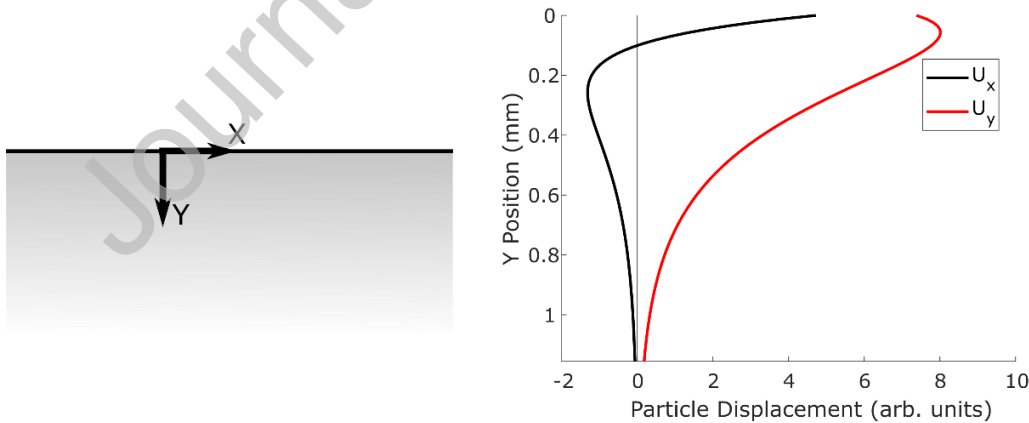


Figure 1. An example displacement profile for a Rayleigh wave at 5 MHz in aluminum.

Other Rayleigh-like waves have also been characterized, like the Love wave [29], the Stoneley wave [30] and the Scholte wave [31]. All these Rayleigh-like waves involved, in some form, an ideal half-space. That is, Love waves are characterized as existing in a domain composed of a layer on a half-space, Stoneley waves are composed of two different half-spaces, and Scholte waves are composed of two different half-spaces where one is a fluid. The presence of these well-known surface waves in experimental literature belies the fact that real-life structures are never ideal half-spaces. There are a variety of phenomena that explain why these surface wave characterizations are still

applicable, if only as approximations, but the phenomena most relevant to the subject of this paper is the existence of quasi-Rayleigh waves.

In a plate waveguide, a surface wave that appears to be a Rayleigh wave can be excited, but it may be more accurate to refer to it as a quasi-Rayleigh wave. Quasi-Rayleigh waves were first characterized by I. Viktorov and R. Grigoryan in 1959 [32] and are actually a superposition of two types of waves present in plate waveguides, the S0 and A0 Lamb wave modes. Lamb waves were first characterized by Horace Lamb in 1917 [33] and can be categorized into symmetric and anti-symmetric modes based on their in-plane displacement. Lamb modes are dispersive and propagate in isotropic, elastic, plate waveguides with traction-free boundary conditions. At higher frequencies, the S0 and A0 modes' dispersion solutions converge onto the Rayleigh wave's wave speed as shown in Figure 2.

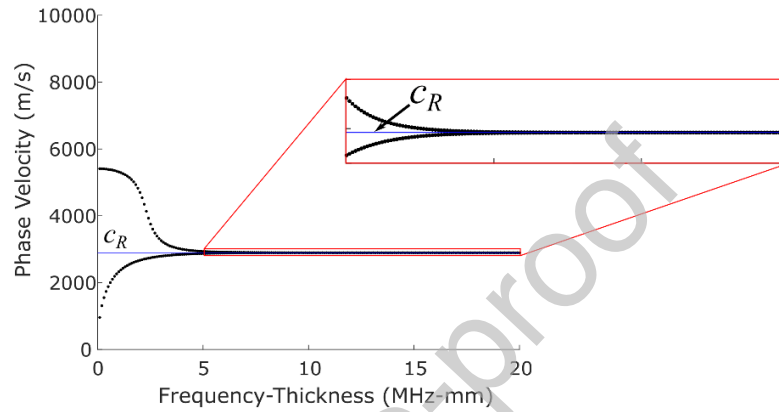


Figure 2. Depiction of the S0 and A0 mode's dispersion solutions converging onto the Rayleigh wave speed. The example dispersion curves were calculated for an aluminum plate waveguide ($\rho=2700 \text{ kg/m}^3$, $E=70\text{GPa}$, $\nu=0.33$). The blue solid line indicates the Rayleigh wave's phase velocity for reference and is not a viable dispersion solution for a finite-thickness waveguide.

Due to the convergence observed in Figure 2, when a practitioner attempts to excite a Rayleigh wave at higher frequencies in a finite-thickness waveguide, both the S0 and A0 Lamb modes will be excited instead of a Rayleigh wave. These two modes will propagate together in the waveguide and their displacement profiles will superpose to form a profile resembling a Rayleigh wave as demonstrated in Figure 3. This resemblance is the reason why this type of wave is referred to as a quasi-Rayleigh wave. Although not shown in Figure 3, it should be noted that the displacement components of a given Lamb mode are typically $\pi/2$ out-of-phase, like a Rayleigh wave, and it is important to incorporate this characteristic when calculating the superposition of the displacement profiles.

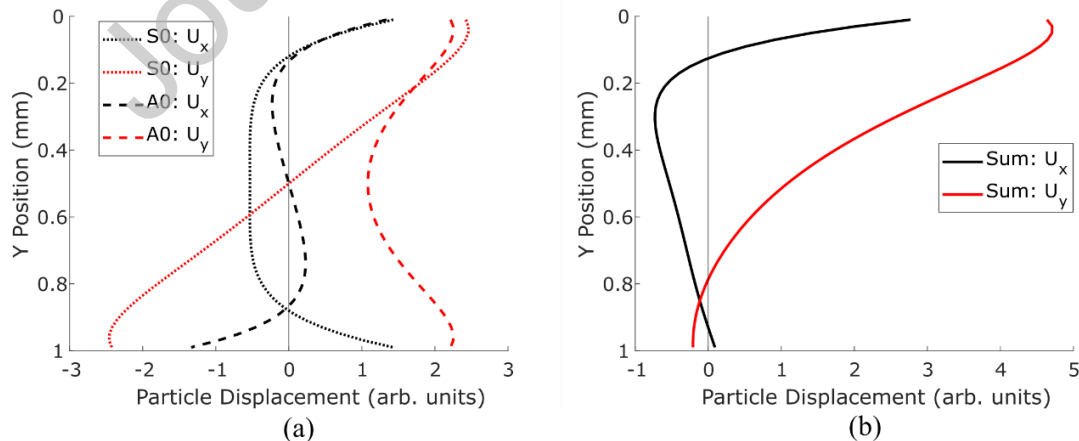


Figure 3. (a) Displacement profiles of the S0 and A0 modes at 5 MHz in a 1-mm thick aluminum plate waveguide. (b) The superposition of the S0 and A0 modes' displacement profiles.

The fact that this superposition leads to a Rayleigh-wave-like displacement profile, can be explained using the partial-wave solutions of the Christoffel equations [34]. That is, when the S0 and A0 modes converge on the Rayleigh wave speed, the partial waves that make up these two guided wave modes and Rayleigh wave are all approximately the same evanescent partial waves. Due to the similarity of the partial waves, when the S0 and A0 modes undergo superposition, the partial waves on one surface destructively interfere while the partial waves on the other surface constructively interfere. This leaves one pair of evanescent partial waves on one surface, which leads to the quasi-Rayleigh wave's Rayleigh-wave-like displacement profile [35].

A consequence of the fact that the frequency and wavenumber are only approximately the same, is that a Rayleigh wave's displacement profile cannot be perfectly represented by the superposition of the S0 and A0 modes. An example of this can be seen by comparing Figure 1 and Figure 3(b). Additionally, for a given frequency, f_o , the slight difference in wavenumber between the S0 and A0 modes creates what is known as a spatial beat phenomenon, where the S0 and A0 modes become out-of-phase with each other as they propagate. This is often characterized in terms of a beat length and can be defined as the propagation distance required for the phase difference between the S0 and A0 modes to reach 2π , thereby completing a "beat" [23, 36].

$$L_B(f = f_o) = \frac{2\pi}{k_{A0} - k_{S0}}. \quad (2)$$

As a consequence of the superposition that we discussed earlier, this beat phenomenon results in quasi-Rayleigh wave energy shifting from one surface to another and then back as depicted in Figure 4.

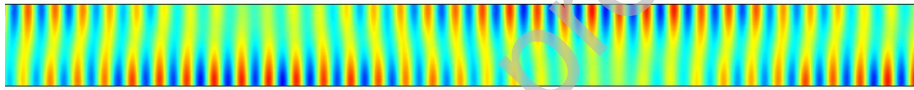


Figure 4. A depiction of the y-component of the displacement of a quasi-Rayleigh wave propagating in an aluminum plate waveguide.

Given the characteristics of a quasi-Rayleigh wave, the waveguide's symmetry is a necessity. The symmetry of the material properties, domain geometry and boundary conditions allow for the formation of the symmetric and anti-symmetric Lamb waves and provides common surfaces for the spatial beat phenomenon to traverse. If we extend this to other surface waves, we find that similar behavior can be observed. For example, if one constructs a symmetric plate waveguide with **aluminum-tungsten-aluminum** layers, a quasi-Stoneley wave solution is theoretically possible [35].

3. METHODS OF MANIPULATING THE QUASI-RAYLEIGH WAVE

From eq. 2, we know that for a given frequency, f_o , the beat length is a function of the S0 and A0 modes' wavenumbers. For a given frequency, the wavenumbers can be altered by changing the thickness or material properties of the plate waveguide. Changing the thickness of the waveguide is the easier of the two methods since the Lamb wave's dispersion curves scale with respect to the thickness of the plate waveguide, which can be represented as shown in Figure 5(a). Presenting the dispersion curves of plate waveguides in this manner is fairly common in the literature (e.g., [37-39]) because it allows readers to more easily use published dispersion curves as reference for their specific application. Using this thickness-scaling property of the Lamb wave dispersion curves and eq. 2, we can plot the beat length as a function of a plate waveguide's thickness. An example plot of the beat length versus the varying thickness of an aluminum plate waveguide is shown in Figure 5(b).

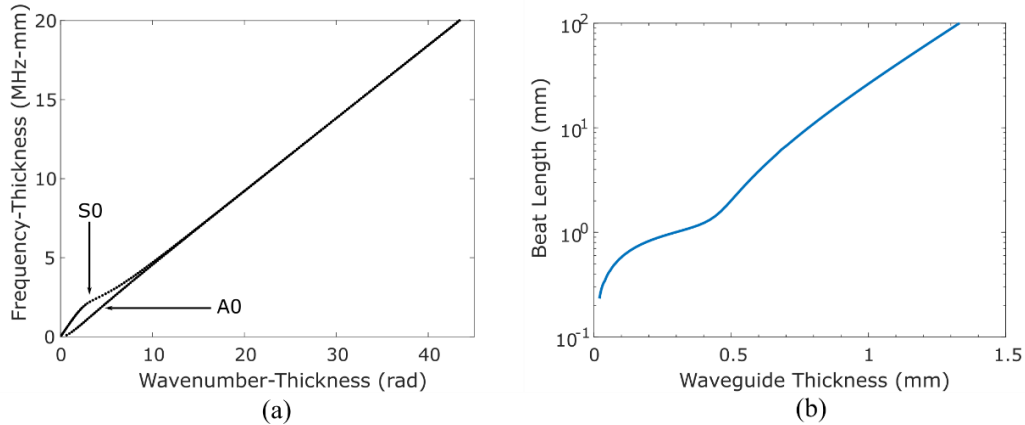


Figure 5. (a) Example of how the dispersion curves for an aluminum plate waveguide ($\rho=2700 \text{ kg/m}^3$, $E=70 \text{ GPa}$, $\nu=0.33$, $c_L=6198 \text{ m/s}$, $c_S=3122 \text{ m/s}$, $c_R=2906 \text{ m/s}$) scale with the thickness of the waveguide when presented as a frequency-versus-wavenumber plot. (b) The resulting beat length plot as a function of waveguide thickness when a frequency of 5 MHz is assumed.

The main trend, shown in Figure 5(b), is that the beat length increases for increasing waveguide thickness. Conversely, by decreasing the waveguide thickness, we can drastically shorten the beat length in localized regions of the plate waveguide and thereby make localized regions with minimal SAW amplitude. These regions will be referred to as Minimal-Amplitude Regions (MAR). The amount of this reduction in amplitude is governed by the frequency-thickness product. At greater frequency-thicknesses, the evanescence of the partial waves will increase which results in wave energy being more focused on a single surface of the waveguide and, as a result, a greater amplitude reduction in the MAR. These basic observations form the basis of our approach to engineer the quasi-Rayleigh wave beat phenomenon. In the following section, we detail how this is exploited to design MARs in a waveguide.

4. DESIGNING MINIMAL-AMPLITUDE REGIONS (MAR) IN PLATE WAVEGUIDES

We present three designs in this section, each of which improves upon the previous design. The rationale for each is described using fundamental concepts of wave mechanics. Numerical simulations are carried out to evaluate and discuss the effectiveness of the designs.

Unlike the wave-scattering-based method designed by Humphreys and Ash [21], the proposed quasi-Rayleigh-wave approach uses an interference-based method which results in minimal scattering and energy loss. Also, the wave mechanics and designs are comparatively simple because complicated patterning of the waveguide surface is avoided. However, changing the thickness of the waveguide does necessitate mode conversion, which we optimize by ensuring that any changes in waveguide thickness are smooth and expected displacement profiles between conversions are similar [40].

4.1. Design 1: Varying the thickness of the single-layer plate waveguide

The first design is the easiest approach and involves simply reducing the thickness of the plate waveguide using a continuous transition as depicted in Figure 6(a).

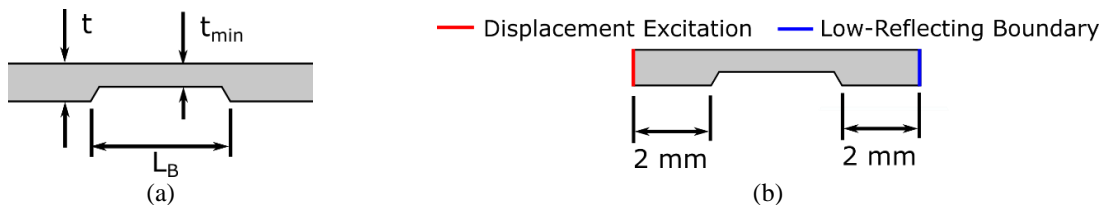


Figure 6. (a) Design 1 which involves decreasing the thickness of the plate waveguide in order to create a MAR. (b) Schematic of the assumptions and dimensions used for the frequency-domain simulation of Design 1.

The width of the thinner region would be equivalent to the beat length, while the minimum thickness, t_{min} , would be determined using a beat-length-versus-thickness plot as shown in Figure 5(b). A frequency-domain simulation of an aluminum plate waveguide ($\rho=2700 \text{ kg/m}^3$, $E=70 \text{ GPa}$, $\nu=0.33$) was setup as shown in Figure 6(b) with $t = 1 \text{ mm}$, $t_{min} = 0.65 \text{ mm}$, and $L_B = 5.1 \text{ mm}$. The displacement excitation uses the Rayleigh wave's displacement profile due to its similarity to the quasi-Rayleigh wave's displacement profile. The results of the frequency-domain simulation are shown in Figure 7. All simulations shown in this paper used COMSOL Multiphysics Finite Element software with a mesh composed of elements no greater than 1/10 of the Rayleigh wave's wavelength (i.e., 10 elements per wavelength). This element size was chosen after checking that the solution remains unchanged at this and smaller element sizes. The mesh itself was composed of triangular elements and the solid mechanics physics module was used. For all of these and other finite-element components, default/built-in COMSOL functions were used. The geometry of the continuous transition that results in the reduction of the thickness is not strictly defined in Figure 6 because we found that small changes to it do not significantly change the behavior of the quasi-Rayleigh wave. Beyond being continuous, the only requirement for the transition is that the reduced thickness is flat and long enough to allow for the beat phenomenon as shown in Figure 7(a).

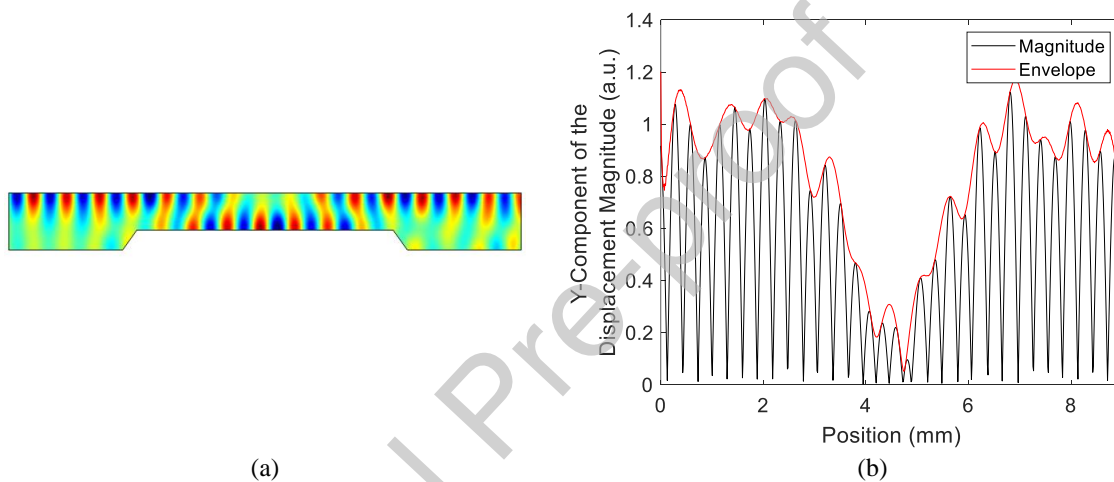


Figure 7. (a) Surface plot of the y-component of the displacement from Design 1's simulation results. (b) Plot of the y-component of the displacement's magnitude on the top surface of the waveguide versus the position. The envelope is the Hilbert transform of the surface displacement's magnitude.

As shown in Figure 7, Design 1 can be used to create a MAR. Figure 7(a) shows that there is no noticeable reflection or scattering from the MAR and that the wave transmits well. The displacement plot in Figure 7(b) shows a decrease in amplitude of about 90.4% and a full-width at half-depth of about 1.8 mm. The decrease in amplitude is significant as expected, however the full-width at half-depth is noticeably less than the beat length. From Figure 7(b), we see that the MAR width is approximately equal to the beat length if we measure from the point where the wave amplitude begins to decrease to the point where the wave amplitude stops increasing. That is, the transfer of wave energy from one surface to the other begins almost immediately once the waveguide is made thinner, but the transfer is gradual which leads to a smaller-than-expected full-width at half-depth. These are characteristics that must be taken into account when considering potential implementations.

Unsurprisingly, the plate waveguide before and after the MAR is just as likely to experience a beat phenomenon as the MAR itself. This is the reason why Design 1's simulation is designed with only 2 mm on either side of the MAR. The beat length for the thick and thin portions of the waveguide can be found using the beat-length-versus-frequency plot shown in Figure 5(b). Although the beat length for a 1-mm thick waveguide is 26.48 mm, which is in excess of 2 mm, we noted previously that it appears that the transfer of wave energy begins immediately. In the case of Design 1's simulation, this means that the wave energy has already started to transfer before encountering the MAR. We have found that if the length before the MAR is made greater than 2 mm then it leads to significant scattering and reflection as the partially transferred wave energy interacts with the MAR. This is demonstrated in Figure 8 where the 2 mm on either side of the MAR was increased to 7 mm.

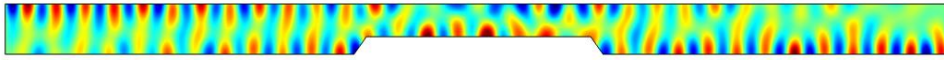


Figure 8. Design 1's simulation but the length of the 1-mm thick waveguide on either side of the MAR was increased to 7 mm from 2 mm shown in Figure 6 and 7. The plot is a surface plot of the **y-component of the displacement**.

In this section, we were able to demonstrate that designing a MAR using the principles of quasi-Rayleigh waves is possible. The decrease in wave amplitude is significant and appears to transmit the wave energy past the MAR. Although the decrease in wave amplitude in the MAR is gradual which leads to a smaller full-width at half-maximum, a wider MAR can be easily designed to account for this by revising the thickness of the waveguide in the MAR. The main problem we identified is that the beat phenomenon is still present outside of the MAR and can render the MAR ineffective as shown in Figure 8. In the following section, we describe another Design that addresses this problem.

4.2. Design 2: Adding a layer to the plate waveguide

To address the problem of a beat phenomenon outside the MAR, we will use concepts from strip waveguides mentioned in Section 1 and observations made at the end of Section 2. The observation being that the beat phenomenon and, as a result, the quasi-Rayleigh wave are only possible because of the symmetry of the waveguide. If the symmetry of the geometry, boundary conditions, or material properties is disrupted **then** the beat phenomenon will no longer occur. One way to do this is to simply add another layer, or a substrate, to the plate waveguide. A similar approach was originally used for strip waveguides.

There are a variety of strip waveguide designs [8-12], but they are typically composed of two materials: a 'slow' material that acts as the 'strip', or finite layer, and a 'fast' material that acts as the substrate. The original purpose of the strip-waveguide design was to redirect wave energy **in the plane of a plate** as opposed to this paper's attempts at redirecting the wave energy **through the thickness**. There are two aspects of the strip waveguide design that allows the wave energy to be focused in the strip as opposed to the substrate; the aforementioned removal of symmetry, and the choice in 'slow' and 'fast' materials. It is stated in Li et al. [12] that "The strip material must be 'slow' relative to that of the substrate..." That is, the Rayleigh wave speed in the strip must be less than the Rayleigh wave speed in the substrate. The reason for this necessary condition can be readily explained using partial wave theory.

From eq. 1, we know that the Rayleigh wave speed is always less than the shear wave speed for all possible Poisson's ratio. Including the longitudinal wave speed, the relative speeds can be summarized as $c_L > c_S > c_R$. This hierarchy is most noticeable when you plot the partial wave solutions of the Christoffel equations in the form of slowness curves. Two versions of these slowness curves are shown in Figure 9, one for the 'slow' layer and the other for the 'fast' substrate. The axes of slowness curves is typically the inverse of the phase velocity and the curves for an isotropic material appear as two concentric circles. The radii of these circles are equal to the inverse of the longitudinal wave speed and the inverse of the shear wave speed. If the inverse phase velocity of a partial wave is outside the radius of the respective circle, then the partial wave is understood to have an evanescent or decaying wave solution. As a result of this, the Rayleigh wave is predictably made up of only evanescent longitudinal and evanescent shear partial waves due to the hierarchy mentioned previously. This composition can be readily confirmed by observing the superposition of decaying terms in the Rayleigh wave displacement solution [28]. From the partial wave theory, we also know that the wavevector component of the partial wave that is parallel to the direction of guided wave propagation must be equivalent to the wavenumber of the guided wave [41]. That is, for a guided wave propagating in the x-direction with wavenumber, k , and frequency, f , all partial waves that make up the guided wave will require that $k_x = k$. This relationship between partial waves and the guided wave they make up are depicted for a two-layer media as shown in Figure 9.

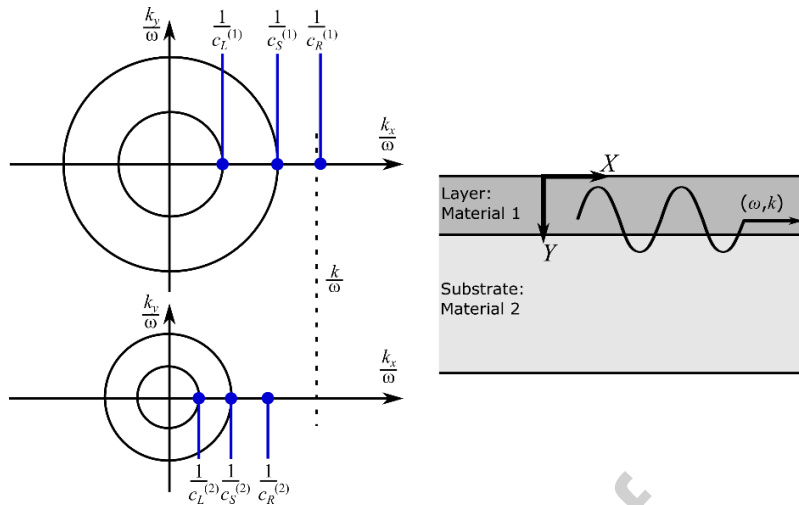


Figure 9. Schematic of slowness curves corresponding with a ‘slow’ layer and a ‘fast’ substrate.

Figure 9 shows the relative slowness curve sizes given a ‘slow’ layer and a ‘fast’ substrate. The ‘fast’ substrate has slowness curves that are smaller circles than the slowness curves of the ‘slow’ layer. This size difference, along with the wavenumber equivalence shown by the dashed line in Figure 9, forces the partial waves in the substrate to be evanescent. In other words, the addition of the ‘fast’ substrate forces an evanescent solution in the substrate which is characteristic of a surface wave and prevents the beat phenomenon by breaking the waveguide’s symmetry. The efficacy of this approach can be confirmed by using the SAFE method to calculate the dispersion curves of the fundamental modes before and after the addition of a ‘fast’ substrate as shown in Figure 10. The waveguide that consists of a ‘slow’ layer and a ‘fast’ substrate will be referred to as the two-layer waveguide from now on. A zoomed-in version that is focused on the ‘slow’ layer’s Rayleigh wave speed is shown in Figure 11(a).

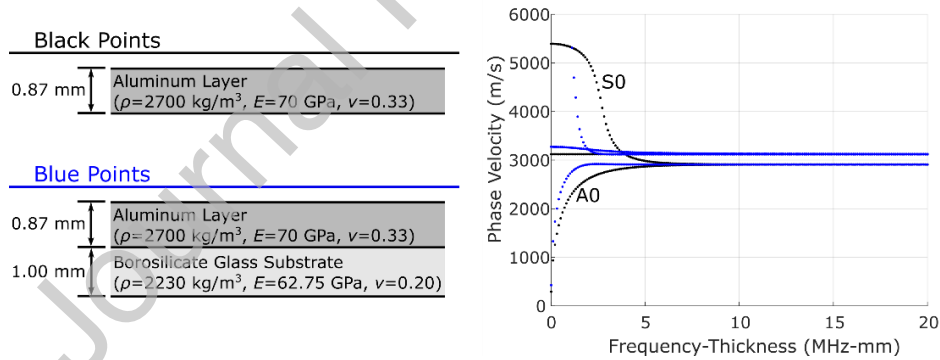


Figure 10. Dispersion curves of the fundamental modes from before and after a ‘fast’ borosilicate glass substrate is added to an aluminum layer. For reference, the aluminum layer has the following wave speeds, $c_L = 6198$ m/s, $c_S = 3122$ m/s, and $c_R = 2906$ m/s, while the borosilicate glass has $c_L = 5592$ m/s, $c_S = 3424$ m/s, and $c_R = 3109$ m/s.

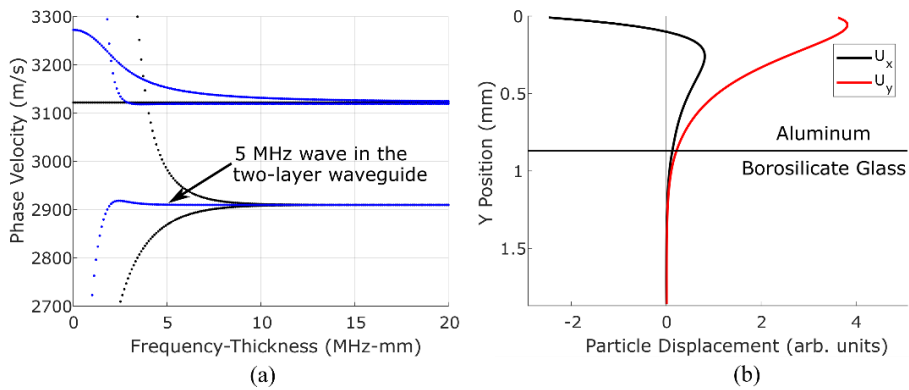


Figure 11. (a) Zoomed-in view of the dispersion curves from Figure 10 that is focused on the aluminum Rayleigh wave speed. (b) Example displacement profile of the fundamental mode (pointed to in (a)) in the two-layer waveguide at 5 MHz.

The Rayleigh wave speed for the aluminum layer and borosilicate glass substrate are about 2906 m/s and 3109 m/s, respectively. In Figure 11(a), the fundamental Lamb modes are the black data points converging at approximately the Rayleigh wave speed in aluminum, while there is a single fundamental mode from the two-layer waveguide that plateaus at the Rayleigh wave speed in aluminum. From this alone, it can be inferred that the superposition of modes necessary for the beat phenomenon is no longer possible in the two-layer waveguide. In Figure 11(b) an example displacement profile of the two-layer waveguide's fundamental mode is shown. The displacement profile is at a frequency of 5 MHz, which is after the two-layer waveguide's dispersion curve has plateaued, and shows a Rayleigh-wave-like displacement profile. The similarity in displacement profile and having approximately the same phase velocity as the Rayleigh wave in aluminum suggests that there would be very good mode conversion between the two-layer waveguide's fundamental mode and the quasi-Rayleigh wave. When combined, the resulting MAR design is as shown in Figure 12. This new design was checked in a frequency-domain simulation that is setup as shown in Figure 12.

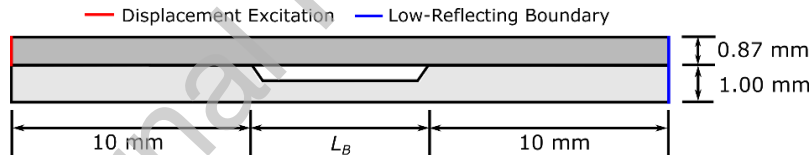
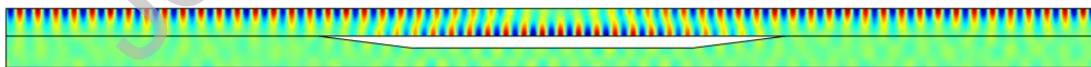


Figure 12. Schematic of the assumptions and dimensions used for the frequency-domain simulation of Design 2.

The thicknesses and material properties will be the same as shown in Figure 10. Using Figure 5(b) again, the beat length for the MAR was designed to have an $L_B = 15.0$ mm. The simulation results are shown in Figure 13.



(a)

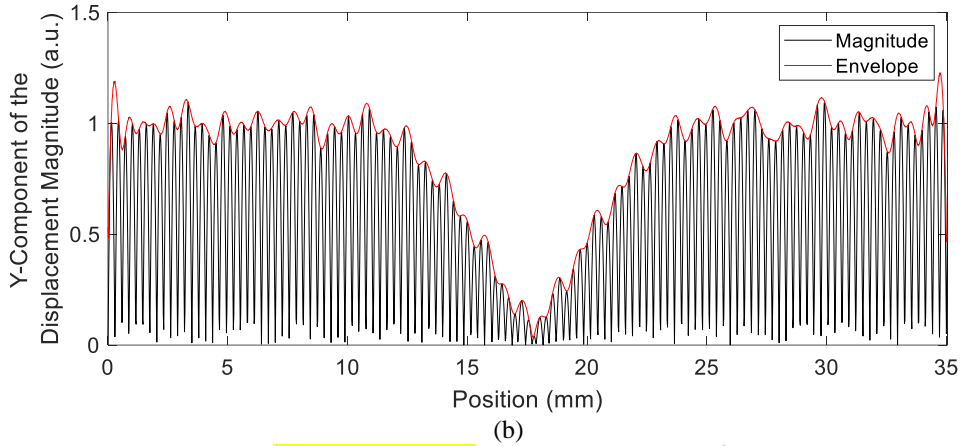
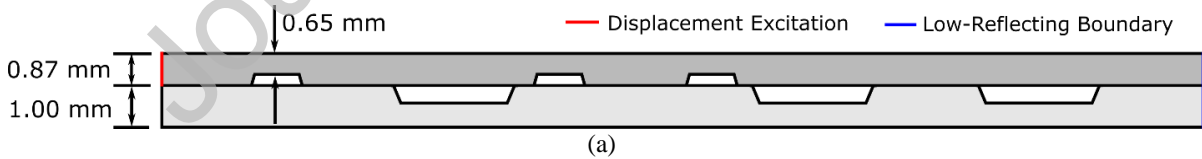


Figure 13. (a) Surface plot of the **y-component of the** displacement from the simulation results. (b) Plot of the y-component of the displacement's magnitude on the top surface of the waveguide versus the position. The envelope is the Hilbert transform of the surface displacement's magnitude.

As shown in Figure 13, this design can also be used to create a MAR. Figure 13(a) shows that not only is there no noticeable reflection or scattering, but that there are no longer any problems with the beat phenomenon occurring in regions outside the MAR. The displacement plot in Figure 13(b) shows a decrease in amplitude of about 96.6% and a full-width at half-depth of about 5.0 mm. The perceived improvement in amplitude decrease is most likely a result of the greater frequency-thickness in the MAR used for this simulation and the perceived improvement in full-width at half-depth is due to the larger beat length. Overall, Design 1 and Design 2 achieve similar performance, while Design 2 is immune to the beat phenomenon outside the MAR.

4.3. Multiple MARs

The true strength of Design 1 and Design 2 are that they are not mutually exclusive and can be combined to achieve consecutive MARs of variable width and spacing. A frequency-domain simulation demonstrating this was done with the setup shown in Figure 14(a). Each MAR design is repeated three times for a total of six MARs. Design-1-based MARs start at 10 mm, 40 mm and 55 mm, while Design-2-based MARs start at 23 mm, 62 mm and 85 mm. Just like in the previous sections, the beat lengths of these MARs are 5.1 mm and 15.0 mm, respectively. The results are shown in Figure 14(b) and suggest similar performance to when there was only a single MAR and the throughput of wave energy is approximately unchanged due to no noticeable scattering or reflections. The third MAR in the series has a noticeably shallow decrease in amplitude, which is most likely due to MARs with smaller frequency-thicknesses having more dissimilar S_0 and A_0 modes which leads to inconsistent interference behavior.



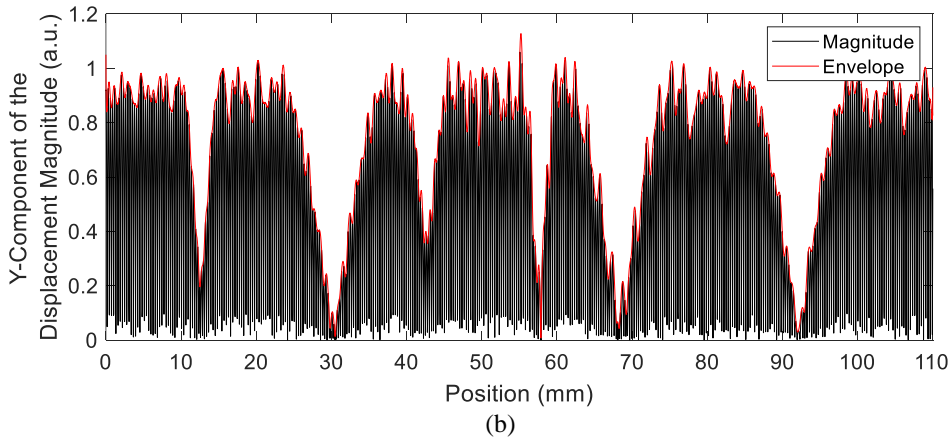


Figure 14. (a) Schematic of the assumptions and dimensions used for the frequency-domain simulation that uses both Design 1 and Design 2. (b) Plot of the **y-component of the** displacement's magnitude on the top surface of the waveguide versus the position. The envelope is the Hilbert transform of the surface displacement's magnitude.

4.4. Frequency range of the MAR

To check the frequency range of a MAR, the Design-2 simulation setup from Section 4.2 is used but a frequency sweep is applied. The MAR is designed for a frequency of 5 MHz but at lower frequencies (e.g., 3 MHz as shown in Figure 15(a)), the beat phenomenon can still be observed. However, it has more scattering after the MAR and unintended beat lengths. **The scattering of high-frequency quasi-Rayleigh waves have been studied before [42].** At frequencies slightly above the design frequency (e.g., 6 MHz as shown in Figure 15(b)), the beat lengths are long enough such that the beat phenomenon is always interrupted. This interruption leads to minimal mode conversion, which results in a significant amount of scattering and reflection. It is not till the frequencies are high enough that the beat lengths are very large (e.g., 8 MHz as shown in Figure 15(c)) does the wave appear to be nearly unaffected by the MAR.

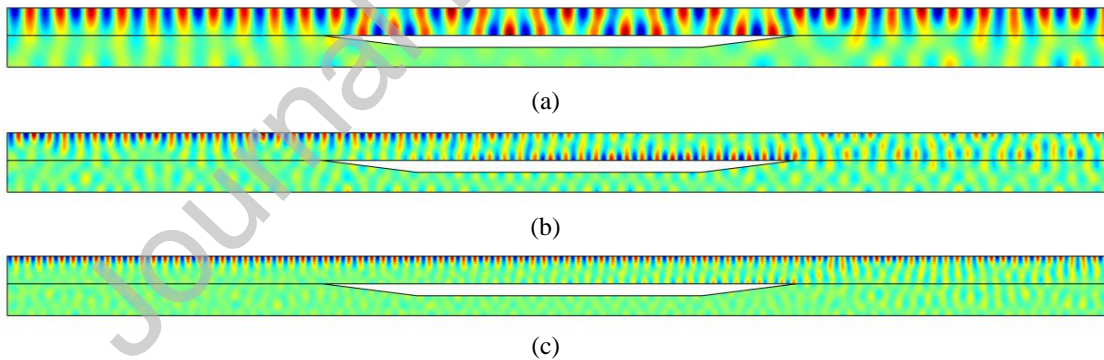


Figure 15. Surface plots of the y-component of the displacement when a 3 MHz, 6 MHz and 8 MHz surface wave is incident upon a Design 2 MAR that was designed for 5 MHz.

To compare these three frequency ranges, we have plotted the beat length as a function of frequency for an aluminum plate that is 0.87-mm thick as shown in Figure 16. Points at approximately 3 MHz, 5 MHz, 6 MHz, and 8 MHz are labeled for reference. Of the frequency ranges, the one of most interest is the one that starts at 8 MHz as shown in Figure 15(c). It is a frequency range in which a MAR becomes “invisible” to the surface wave. Unfortunately, outside of simulations with parametric studies, there is currently no clear method to determine the frequency at which this “invisibility” begins.

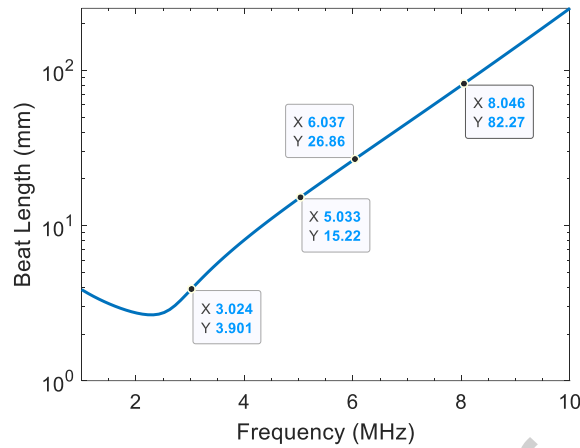


Figure 16. Beat length versus frequency of an aluminum plate with a thickness of 0.87 mm. Several data labels are provided as context for the frequency ranges shown in Figure 15.

5. POTENTIAL IMPLEMENTATIONS

Due to the simplicity of the wave phenomenon and the quality of the result, we can quickly devise several implementations of the MAR designs that may be applicable to a variety of fields. Three potential implementations are depicted in Figure 17.

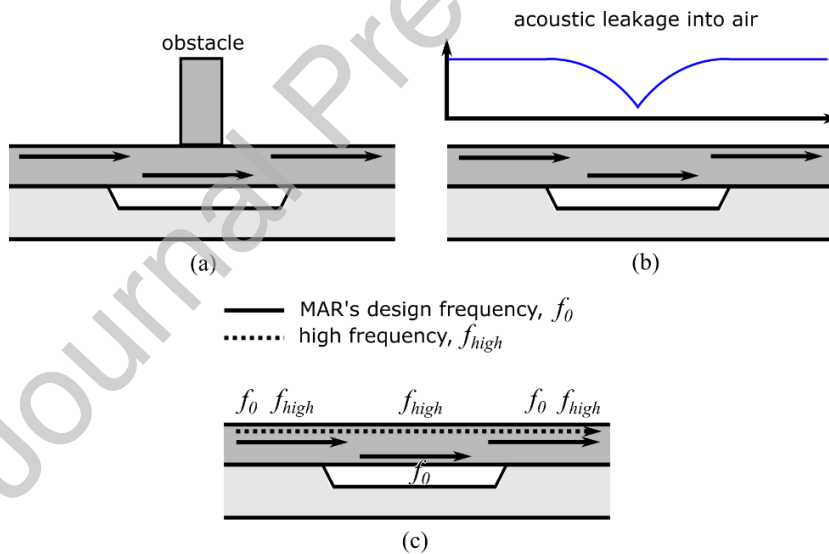


Figure 17. Schematics of how the MAR design could be used to (a) avoid surface obstacles, (b) make regions with minimal acoustic leakage, and (c) localized high-pass filter.

Figure 17(a) depicts an obstacle present on the surface of the layer that would usually cause an incident surface wave to experience significant scattering and reflection. However, the wave energy avoids the obstacle by using the MAR. Depending on the application, this obstacle could be a support structure, weld, or the wall of a sealed chamber. This implementation works because surface wave energy is focused on the layer's bottom surface in the MAR, which makes the wave much less susceptible to changes in boundary condition and/or domain on the layer's top surface.

There are some applications of SAWs that use the acoustic leakage emitted from them. Figure 17(b) depicts how the MAR can be used to create regions with minimal acoustic leakage. In this and other implementations, it is important

to remember that symmetry is important for the beat phenomenon. The top and bottom surfaces in the MAR region should be in contact with the same type of medium (i.e., water, air, etc.) for optimal performance.

The final implementation shown in Figure 17(c) is based on the frequency range of the MAR. Since the MAR will be “invisible” at certain high frequencies, the MAR can locally separate the frequency the MAR was designed for and the high frequencies that are not affected by the MAR. These high frequencies could be noise that would be removed in post-processing, or harmonics that develop due to various phenomena.

6. CONCLUSION

In this paper, we discussed two designs that can be used separately or in combination to construct localized regions with minimal surface wave amplitude, also referred to in the paper as MAR. The MAR designs are simple, can be adjusted to have variable width and can be placed consecutively due to minimal energy loss from scattering and reflection. These favorable characteristics are achieved by exploiting the quasi-Rayleigh wave’s beat phenomenon, which is inherently an interference-based phenomenon that consists of very little wave scattering or reflection. However, what makes this approach viable is the addition of a second layer that draws on concepts from strip waveguides to improve stability and performance. These iterative improvements are visible in the multiple MAR designs (i.e., Figure 8, Figure 12, Figure 14) discussed in this paper. A detailed explanation of the physics and other details pertinent to each design are provided and simulations were used to determine their efficacy.

Overall, the results of the simulations demonstrate that the designs are capable of constructing MARs with low transmission loss and a high reduction in local wave amplitude (often >90%). Even with multiple MARs of different widths and placed at various distances, the MAR designs perform well. Additionally, it was found that if the frequency is high enough, the surface wave is not noticeably affected by the MAR. Lastly, three potential ways of implementing the MAR designs were discussed. These implementations were chosen based on the current SAW applications that were mentioned in the introduction, this includes SHM/NDE, acoustofluidics, and SAW-based RF devices (e.g., information storage devices). Experiments are being considered but are likely to introduce a large variety of new variables to consider (e.g., effect of beam width relative to MAR width, dimensions/geometry in the third dimension, oblique incidence to the MAR, etc.). Based on this, we have determined that a 3D analysis and experiment would be better suited as a future, stand-alone paper.

Declaration of Competing Interests

The authors declare that they have no known competing financial interests or personal relationships that could have appeared to influence the work reported in this paper.

ACKNOWLEDGEMENT

We acknowledge the support of Los Alamos National Laboratory’s Laboratory Directed Research and Development Early Career Research program under the grant LDRD20190568ECR.

References

- [1] J. Friend and L. Y. Yeo, "Microscale acoustofluidics: Microfluidics driven via acoustics and ultrasonics," *Rev. Mod. Phys.*, vol. 83, no. 2, pp. 647-704, 2011.
- [2] C. Ruppel, "Acoustic Wave Filter Technology - A Review," *IEEE Trans. Ultrason. Ferroelectr. Freq. Control*, vol. 64, no. 9, pp. 1390-1400, 2017.
- [3] V. P. Plessky and L. M. Reindl, "Review on SAW RFID Tags," *IEEE Trans. Ultrason. Ferroelectr. Freq. Control*, vol. 57, no. 3, pp. 654-668, 2010.
- [4] R. White and F. Voltmer, "Direct Piezoelectric Coupling to Surface Elastic Waves," *Applied Physics Letters*, vol. 7, no. 12, pp. 314-316, 1965.
- [5] H. Yatsuda, "Design Techniques for SAW Filters Using Slanted Finger Interdigital Transducers," *IEEE Trans. Ultrason. Ferroelectr. Freq. Control*, vol. 44, no. 2, pp. 453-459, 1997.
- [6] W. R. Smith, H. M. Gerard and W. R. Jones, "Analysis and Design of Dispersive Interdigital Surface-Wave Transducers," *IEEE Trans. Micro. , Vols. MTT-20*, no. 7, pp. 458-471, 1972.
- [7] T.-T. Wu, H.-T. Tang, Y.-Y. Chen and P.-L. Liu, "Analysis and Design of Focused Interdigital transducers," *IEEE Trans. Ultrason. Ferroelectr. Freq. Control*, vol. 52, no. 8, pp. 1384-1392, 2005.
- [8] H. Seidel and D. White, "Ultrasonic Surface Waveguide". United States of America Patent 3,406,358, 15

October 1968.

- [9] L. R. Adkins and A. J. Hughes, "Investigations of Surface Acoustic Wave Directional Couplers," *IEEE Trans. Sonics Ultrason.*, Vols. SU-19, no. 1, pp. 45-58, 1972.
- [10] K. Yen and A. Oliner, "The strip acoustic surface waveguide: Comparison between measurement and theory," *Applied Physics Letters*, vol. 28, no. 7, pp. 368-370, 1976.
- [11] L. R. Adkins and A. J. Hughes, "Elastic Surface Waves Guided by Thin Films: Gold on Fused Quartz," *IEEE Trans. Microwave Theory Tech.*, Vols. MTT-17, no. 11, pp. 904-911, 1969.
- [12] R. C. Li, A. A. Oliner and H. L. Bertoni, "Microwave Network Analyses of Surface Acoustic Waveguides - I. Flat Overlay Guides," *IEEE Trans. Sonics Ultrason.*, Vols. SU-24, no. 2, pp. 66-78, 1977.
- [13] S. Markman, R. C. Li, A. A. Oliner and H. L. Bertoni, "Microwave Network Analyses of Surface Acoustic Waveguides - II. Rectangular Ridge Guides," *IEEE Trans. Sonics Ultrason.*, Vols. SU-24, no. 2, pp. 79-87, 1977.
- [14] H. Tiersten, "Elastic Surface Waves Guided by Thin Films," *J. Appl. Phys.*, vol. 40, no. 2, pp. 770-789, 1969.
- [15] H. Sabine and P. Cole, "Surface acoustic waves in communications engineering," *Ultrasonics*, vol. 9, no. 2, pp. 103-113, 1971.
- [16] V. P. Plessky and A. W. Simonian, "Rayleigh wave reflection and scattering on a resonator," *Phys. Lett. A*, vol. 155, no. 4,5, pp. 281-284, 1991.
- [17] J. Eliason, A. Vega-Flick, M. Hiraiwa, A. Khanolkar, T. Gan, N. Boechler, N. Fang, K. Nelson and A. Maznev, "Resonant attenuation of surface acoustic waves by a disordered monolayer of microspheres," *Appl. Phys. Lett.*, vol. 108, no. 6, p. 061907, 2016.
- [18] S. Alan, A. Allam and A. Erturk, "Programmable mode conversion and bandgap formation for surface acoustic waves using piezoelectric metamaterials," *Appl. Phys. Lett.*, vol. 115, no. 9, p. 093502, 2019.
- [19] V. Laude, M. Wilm, S. Benchabane and A. Khelif, "Full band gap for surface acoustic waves in a piezoelectric phononic crystal," *Phys. Rev. E*, vol. 71, no. 3, p. 036607, 2005.
- [20] T.-W. Liu, Y.-C. Lin, Y.-C. Tsai, T. Ono, S. Tanaka and T.-T. Wu, "Evidence of a Love wave bandgap in a quartz substrate coated with a phononic thin layer," *Appl. Phys. Lett.*, vol. 104, no. 18, p. 181905, 2014.
- [21] R. F. Humphryes and E. A. Ash, "Acoustic Bulk-Surface-Wave Transducer," *Electron. Lett.*, vol. 5, no. 9, pp. 175-176, 1969.
- [22] B. Masserey and P. Fromme, "On the reflection of coupled Rayleigh-like waves at surface defects in plates," *J. Acoust. Soc. Am.*, vol. 123, no. 1, pp. 88-98, 2008.
- [23] B. W. Ti, W. D. O'Brien and J. G. Harris, "Measurements of coupled Rayleigh wave propagation in an elastic plate," *J. Acoust. Soc. Am.*, vol. 102, no. 3, pp. 1528-1531, 1997.
- [24] B. Masserey, E. Kostson and P. Fromme, "Defect detection in multi-layered structures using high frequency guided waves," in *Rev. Prog. Q.*, Burlington, 2011.
- [25] B. Masserey, C. Raemy, P. Fromme, "High-frequency guided ultrasonic waves for hidden defect detection in multi-layered aircraft structures," *Ultrasonics*, vol. 54, no. 7, pp. 1720-1728, 2014.
- [26] C. Jayaraman, C. V. Krishnamurthy, and K. Balasubramaniam, "Higher order modes cluster (HOMC) guided waves – a new technique for NDT inspection," *AIP Conf. Proc.*, vol. 1096, no. 1, 2009.
- [27] L. Rayleigh, "On Waves Propagated along the Plane Surface of an Elastic Solid," *P. Lond. Math. Soc.*, Vols. s1-17, no. 1, pp. 4-11, 1885.
- [28] I. A. Viktorov, *Rayleigh and Lamb Waves*, New York: Springer Science+Business Media, LLC, 1967.
- [29] A. E. H. Love, *Some problems of geodynamics; being an essay to which the Adams prize in the University of Cambridge was adjudged in 1911*, Cambridge: Cambridge University Press, 1911.
- [30] R. Stoneley, "Elastic Waves at the Surface of Separation of Two Solids," *P. R. Soc. London*, vol. 106, no. 738, pp. 416-428, 1924.
- [31] J. Scholte, "The range of existence of Rayleigh and Stoneley waves," *Geophys. J. Int.*, vol. 5, no. s5, pp. 120-126, 1947.
- [32] I. Viktorov and R. Grigoryan, "Quasi-Rayleigh waves in an elastic layer," *Akusticheskij Zhurnal*, vol. 5, no. 3, pp. 171-175, 1959.
- [33] H. Lamb, "On waves in an elastic plate," *P. R. Soc. London*, vol. 93, no. 648, pp. 114-128, 1917.
- [34] C. Hakoda and C. J. Lissenden, "Comparison of quasi-Rayleigh waves and Rayleigh waves, and clarifying the cut-off frequency of quasi-Rayleigh waves," *Ultrasonics*, vol. 92, pp. 50-56, 2019.
- [35] C. Hakoda, "Extending the Applicability of the Partial Wave Method for Interpreting Waves in Elastodynamic Waveguides," Pennsylvania State University, University Park, 2019.
- [36] L. Brekhovskikh and V. Goncharov, "Waves in Plates," in *Mechanics of Continua and Wave Dynamics*, Springer-Verlag, Berlin, Heidelberg, 1994, pp. 79-81.
- [37] R. D. Mindlin and J. Yang, *Introduction to the mathematical theory of vibrations of elastic plates*, World

Scientific Publishing Co. Pte. Ltd, 2006.

[38] J. L. Rose, *Ultrasonic Waves in Solid Media*, Cambridge: Cambridge University Press, 1999.

[39] J. Achenbach, *Wave Propagation in Elastic Solids*, Amsterdam: North-Holland Publishing Company, 1976.

[40] P. Puthillath, J. M. Galan, B. Ren, C. J. Lissenden and J. L. Rose, "Ultrasonic guided wave propagation across waveguide transitions: energy transfer and mode conversion," *J. Acoust. Soc. Am.*, vol. 133, no. 5, pp. 2624-33, 2013.

[41] L. P. Solie and B. A. Auld, "Elastic waves in free anisotropic plates," *J. Acoust. Soc. Am.*, vol. 54, pp. 50-65, 1973.

[42] B. Masserey and P. Fromme, "Analysis of high frequency guided wave scattering at a fastener hole with a view to fatigue crack detection," *Ultrasonics*, vol. 76, pp. 78-86, 2017.

Journal Pre-proof